Spin, charge, and orbital correlations in the one-dimensional t_{2g}-orbital Hubbard model

J. C. Xavier,[1,2] H. Onishi,[3] T. Hotta,[3] and E. Dagotto[1]
[1]*Condensed Matter Sciences Division, Oak Ridge National Laboratory, Oak Ridge, Tennessee 37831, USA and Department of Physics, The University of Tennessee, Knoxville, Tennessee 37996, USA*
[2]*Universidade Estadual Paulista, CP 713, 17015-970 Bauru, SP, Brazil*
[3]*Advanced Science Research Center, Japan Atomic Energy Research Institute, Tokai, Ibaraki 319-1195, Japan*
(Received 4 July 2005; revised manuscript received 14 October 2005; published 10 January 2006)

We present the zero-temperature phase diagram of the one-dimensional t_{2g}-orbital Hubbard model, obtained using the density-matrix renormalization group and Lanczos techniques. Emphasis is given to the case of the electron density $n=5$ corresponding to five electrons per site, while several other cases for electron densities between $n=3$ and 6 are also studied. At $n=5$, our results indicate a first-order transition between a paramagnetic (PM) insulator phase, with power-law slowly decaying correlations, and a fully polarized ferromagnetic (FM) state by tuning the Hund's coupling. The results also suggest a transition from the $n=5$ PM insulator phase to a metallic regime by changing the electron density, either via hole or electron doping. The behavior of the spin, charge, and orbital correlation functions in the FM and PM states are also described in the text and discussed. The robustness of these two states against varying parameters suggests that they may be of relevance in quasi-one-dimensional Co-oxide materials, or even in higher dimensional cobaltite systems as well.

DOI: 10.1103/PhysRevB.73.014405 PACS number(s): 75.30.Kz, 71.10.Fd, 75.50.Cc, 75.10.−b

I. INTRODUCTION

The study of the exotic properties of cobalt oxides is an exciting area of investigation that is currently attracting considerable attention in the research field of condensed-matter physics. Among the main reasons for this wide effort, the recent discovery of superconductivity in layered two-dimensional triangular lattices of Co atoms with the composition Na_xCoO_2 has certainly triggered a rapid increase of research activities on cobalt oxides. This material becomes superconducting after H_2O is intercalated,[1] while Na_xCoO_2 exhibits several other competing tendencies, such as charge-ordered insulating, as well as metallic states with varying the Na composition.[2] Furthermore, an incommensurate spin-density wave state has also been observed in this compound and in the related compound $[Ca_2CoO_3]_{0.62}[CoO_2]$.[3] The existence of such a rich phase diagram is a characteristic of strongly correlated electron systems, where complex behavior typically emerges due to the presence of competing states that have similar energies but vastly different transport and magnetic properties.[4]

Furthermore, the magnetic behavior of quasi-one-dimensional Co oxides $A_{n+2}B'B_nO_{3n+3}$ (A=Ca, Sr, Ba, B' and B=Co) has also attracted much attention.[5] For instance, in the $n\rightarrow\infty$ compound $BaCoO_3$, face-sharing CoO_6 octahedra form one-dimensional cobalt chains in which the Co^{4+} ions are in a low-spin state with $S=1/2$. It has been reported that there occurs ferromagnetic (FM) order along the chain below 53 K and a two-dimensional antiferromagnetic (AFM) transition at 15 K due to interchain AFM interactions. The electronic structure has been investigated by *ab initio* calculations,[6] showing that a FM state with an intrachain alternating orbital ordering is the most stable solution. However, in general, the microscopic mechanisms for the appearance of particular spin and orbital configurations in Co oxides is not fully understood, even in relatively simple one-dimensional systems, because of the complexity originating from multiple degrees of freedom.

In such a circumstance, the theoretical study of models for Co oxides is timely and needed to guide further experimental developments. *Ab initio* calculations have already provided important information about Na_xCoO_2 (Ref. 7) as well as $BaCoO_3$ (Ref. 6), and the inclusion of many-body effects is the natural next step. Previous theoretical studies of Co-based systems, including Coulombic repulsion, have mainly focused on triangular lattices. In this context, recent Monte Carlo investigations unveiled the presence of magnetic correlations.[8] Fluctuation-exchange approximations also revealed tendencies toward ferromagnetism and possible triplet-pairing instabilities in a multiorbital model.[9] Several approximate studies of *t-J* (Ref. 10) and single-band Hubbard models[11] have also been presented. To further gain deep insight into the behavior of complex oxides, it is quite important to clarify possible ordering tendencies among the various competing states, stabilized as electron density and coupling are modified. But, unfortunately, this task is difficult due to a lack of reliable unbiased analytical techniques.

In this paper, the first effort toward a detailed numerical analysis of models for cobaltites is presented. We perform a systematic study of a one-dimensional multiorbital Hamiltonian, exploring, in detail, the coupling and electron-density parameter space, by using computationally exact techniques. This level of accuracy is achieved through the use of reliable methods, such as the density-matrix renormalization group (DMRG)[12] and the Lanczos techniques.[13] Although there are already quasi-one-dimensional Co-oxide materials with interesting properties to compare with our results, we also envision this effort as a first step toward a systematic computational analysis of more complicated quasi-two-dimensional triangular-lattice systems.

The organization of this paper is as follows. In Sec. II, the multiorbital model is introduced and the many-body computational techniques used here are briefly discussed. In Sec.

III, the main results are presented. These results are organized based on the observable studied. First, the $n=5$ phase diagram is discussed, where n denotes the number of electrons per site. Then, the spin correlations are presented at several values of n. This is followed by the charge and orbital correlations. Finally, conclusions are presented in Sec. IV. The main result of the paper is the clear dominance of two rather different ground states: (i) a FM state and (ii) a PM state with short-range correlations. Both are found to be very robust against varying couplings and densities, and for this reason, we believe they should be of relevance in real materials.

II. MODEL AND TECHNIQUE

In the investigation reported in this paper, we consider a three-orbital Hubbard model, defined on a one-dimensional chain along the x axis with L sites. The three orbitals represent the t_{2g} orbitals of relevance for cobaltites. The model Hamiltonian is given by

$$H = -\sum_{j,\gamma,\gamma',\sigma} t_{\gamma,\gamma'}(d^{\dagger}_{j,\gamma\sigma}d_{j+1,\gamma'\sigma} + \text{H.c.}) + U\sum_{j,\gamma}\rho_{j,\gamma\uparrow}\rho_{j,\gamma\downarrow} + \frac{U'}{2}\sum_{j,\sigma,\sigma',\gamma\neq\gamma'}\rho_{j,\gamma\sigma}\rho_{j,\gamma'\sigma'} + \frac{J}{2}\sum_{j,\sigma,\sigma',\gamma\neq\gamma'} d^{\dagger}_{j,\gamma\sigma}d^{\dagger}_{j,\gamma'\sigma'}d_{j,\gamma\sigma'}d_{j,\gamma'\sigma} + \frac{J'}{2}\sum_{j,\sigma\neq\sigma',\gamma\neq\gamma'} d^{\dagger}_{j,\gamma\sigma}d^{\dagger}_{j,\gamma\sigma'}d_{j,\gamma'\sigma'}d_{j,\gamma'\sigma}, \quad (1)$$

where the index j denotes the site of the chain; γ indicates the orbitals xy, yz, and zx; and σ is the z component of the spin. The rest of the notation is standard. The hopping amplitudes are $t_{xy,xy}=t_{zx,zx}=t=1$, and zero for the other cases. These simple values for the hopping amplitudes can be easily derived from the overlap of d_{xy}, d_{yz}, and d_{zx} orbitals between nearest-neighbor sites along the x axis. The interaction parameters U, U', J, and J' are the standard ones for multiorbital Hamiltonians, and a detailed description can be found in Ref. 14. These couplings are not independent, but they satisfy the well-known relations $J'=J$ and $U=U'+2J$, due to the reality of the wave function and the rotational symmetry in the orbital space.

We investigate the model described above mainly using the DMRG technique with open boundary conditions.[12] The finite-system algorithm is employed for sizes up to $L=48$, keeping up to $m=350$ states per block. The truncation errors are kept around 10^{-5} or smaller. The center blocks in our DMRG procedure are composed of 64 states due to the three orbitals. Note that, for instance, the t-J model has only three states in these center blocks. As a consequence, keeping $m=350$ states per block in the t_{2g}-orbital Hubbard model is analogous to keeping $m\sim 7000$ states per block in the t-J model.

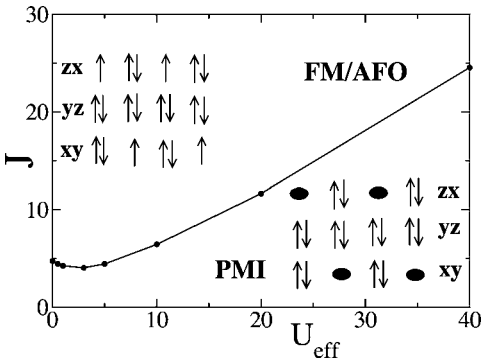

FIG. 1. Ground-state phase diagram for the one-dimensional three-orbital Hubbard model for the electron density $n=5$, using a six-site chain. FM and PMI denote the regions with ferromagnetism and paramagnetism (insulator), the latter with robust short-range correlations, respectively. We also present a schematic picture of the electron configurations. AFO indicates the staggered population of orbitals in the FM state. The reader should consult the text for more details, as well as Fig. 2.

III. RESULTS

A. Phase diagram for density $n=5$

In Fig. 1, we present the ground-state phase diagram for the electron density $n=5$ in the (U_{eff},J) plane with $U_{\text{eff}}=U'-J$. This phase diagram is obtained by comparing the lowest energies for different sectors of the z component of the total spin, S^z_{total}, for $L=6$. For large J, there appears a fully polarized FM phase. On the other hand, for small J, we find a regime characterized by minimum total spin. For simplicity, we refer to this regime as the PM phase, although the results of the spin correlations suggest quantum critical behavior, i.e., quasi-long-range order, as discussed later. Then, this PM phase has robust correlations at short distances.

Let us try to explain the boundary curve without detailed calculations. The phase boundary in the large U_{eff} region is understood from the competition betweem FM and AFM states in the nearest-neighbor sites, leading to $J=U_{\text{eff}}/\sqrt{3}$ in the second-order perturbation in terms of t. If we further expand the phase diagram, even including the unphysical region of $U_{\text{eff}}<0$ (which is only of theoretical interest), we obtain another boundary line, given by $J-U'\sim W$, where W is the bandwidth. Along the line $U_{\text{eff}}=0$ $(U'=J)$, at some critical point $J=J_c$, the PM phase turns into a FM phase. In the FM phase in the region of $U_{\text{eff}}<0$, the system is described by the attractive Hubbard model with the interaction $-U_{\text{eff}}$, if we express the orbital degree of freedom as a pseudospin. Thus, in this rough argument, when the magnitude of the interaction becomes of the order of the bandwidth, $|U_{\text{eff}}|\sim W$, the FM phase without double-occupancy changes to a charge-ordered insulating phase with a periodic array of double-occupied sites, to gain energy using the on-site attraction. For the region of small U_{eff} and J, those two boundary lines may lose their physical meaning, but we can easily imagine that the phase boundary curve is obtained by smoothly connecting the two lines, $J=U_{\text{eff}}/\sqrt{3}$ and $U_{\text{eff}}=-W$, so as to pass through the point $(U_{\text{eff}},J)=(0,J_c)$. Then, we can intuitively understand the shape of the phase boundary curve in Fig. 1.

Note that the phase diagram obtained here has similarities with that already reported by two of the authors at $n=4$ in the context of spin-1 Haldane chains.[15] Note also that the phase diagram in Fig. 1 is obtained by calculations for $L=6$, but other several values of L are also studied. It was observed that for $L=4$, 6, 8, and 10, in the PM regime the ground state has total spin 0, 1, 0, and 1, respectively, for a large set of couplings investigated. As a consequence, it is reasonable to assume that the transition line separates two regions with the minimum and maximum total spin, without intermediate partially polarized regimes.

As described later, our results for the spin, charge, and orbital correlations suggest, roughly, an electron distribution schematically presented in Fig. 1. The electron configuration in the FM phase is quite simple: five electrons per site with a polarized net spin 1/2, and antiferro-orbital (AFO) correlations along the chain. The yz orbital is fully occupied, since there is no electron hopping for this orbital and it is favorable to gain kinetic energy by introducing holes into the itinerant xy and zx orbitals. The existence of FM correlations is a direct consequence of the multiorbital nature of the model and the robust value of J in the FM regime. Namely, when we consider the subspace with five electrons per site and take into account the electron hopping using second-order perturbation theory, it is favorable to form a parallel spin configuration in an intermediate state due to the large value of J.

On the other hand, a more complex electron configuration emerges in the PM phase. The meaning of the full circles in the inset of Fig. 1 for the PM phase is to denote either a spin up or a spin down. Note, however, that quantum fluctuations are strong enough to destroy rigid spin configurations, and the spin arrangement shown in Fig. 1 is just a guidance. To gain insight into the ground-state wave function, it is useful to consider the case of a four-site chain, where results can be obtained exactly by using the Lanczos method. In the strong-coupling limit $U_{\mathrm{eff}} \gg J \gg 1$ [or, more precisely, $1/(U'-J) \ll 1$], it is found that the most important portion of the ground-state wave function is expressed as

$$|\psi\rangle = \frac{1}{\sqrt{24}} \sum_{\mathrm{P}} (-1)^{n_{\mathrm{P}}} \begin{pmatrix} \uparrow\downarrow \\ \uparrow\downarrow \\ \downarrow \end{pmatrix} \otimes \begin{pmatrix} \downarrow \\ \uparrow\downarrow \\ \uparrow\downarrow \end{pmatrix} \otimes \begin{pmatrix} \uparrow\downarrow \\ \uparrow\downarrow \\ \uparrow \end{pmatrix} \otimes \begin{pmatrix} \uparrow \\ \uparrow\downarrow \\ \uparrow\downarrow \end{pmatrix}, \tag{2}$$

where the sum is taken over the permutations of the four spinors and n_{P} is the number of permutations we have to perform to recover the original configuration. Namely, the electron configuration presented in the PM phase of Fig. 1 should be regarded as the equivalent states composed of the four spinors. Note that this is not a rigid configuration, but all permutations are equally important at small J. In particular, all 24 states have the same weight in the ground state at $J=0$, while at finite J, the 24 states are split into three classes with eight states for each, as shown in Fig. 2. Note that each of these classes lead to a distinct peak position in the spin and orbital structure factors. When the peak positions in these channels are denoted by q_{spin} and q_{orbital}, the class (a) has $q_{\mathrm{spin}}=\pi/2$ and $q_{\mathrm{orbital}}=\pi$, class (b) $q_{\mathrm{spin}}=\pi/2$ and $q_{\mathrm{orbital}}=\pi/2$, and class (c) $q_{\mathrm{spin}}=\pi$ and $q_{\mathrm{orbital}}=\pi/2$.

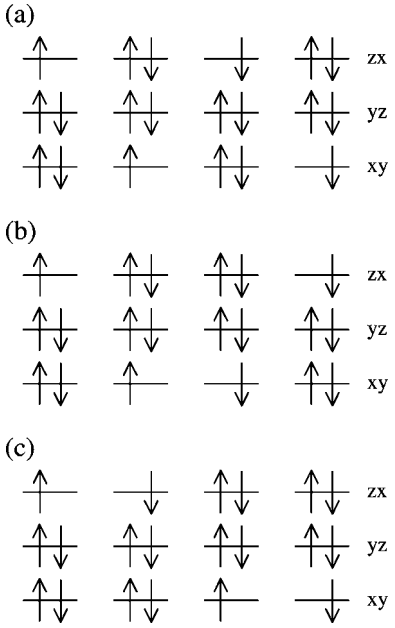

FIG. 2. States with the largest weight in the ground state of a four-site chain solved exactly. Note that each state has eightfold degeneracy. At $J=0$, these three states have the same weight. On the other hand, for nonzero J, the state (a) (and its eightfold degenerate states) has the largest weight, with a spin (orbital) structure factor peaked at $\pi/2$ (π). The states (b) and (c) (each one also with degeneracy 8) have the second- and third-largest weights, respectively, for nonzero J.

We should note that a similar representation of the ground-state wave function for four sites has been found for the $SU(4)$ spin-orbital model.[16] In fact, these two models are related to each other as follows. Since the yz orbital is fully occupied in our studies, the t_{2g}-orbital Hubbard model can be regarded as a two-orbital Hubbard model composed only of xy and zx orbitals. Note that for this two-orbital model, the hopping amplitudes are symmetric and there is no off-diagonal elements. Then, taking a second-order perturbation with respect to electron hopping into consideration, we obtain an effective Hamiltonian in the strong-coupling limit of the form

$$H_{\mathrm{eff}} = \sum_i \tilde{H}_{i,i+1},$$

$$\begin{aligned}
\tilde{H}_{i,j} = & -\frac{4t^2}{U'-J}\left(\frac{3}{4}+\mathbf{S}_i\cdot\mathbf{S}_j\right)\left(\frac{1}{4}-\mathbf{T}_i\cdot\mathbf{T}_j\right) \\
& -\frac{4t^2}{U'+J}\left(\frac{1}{4}-\mathbf{S}_i\cdot\mathbf{S}_j\right)\left(\frac{1}{4}+\mathbf{T}_i\cdot\mathbf{T}_j-2T_i^{\zeta}T_j^{\zeta}\right) \\
& -\frac{4t^2}{U-J'}\left(\frac{1}{4}-\mathbf{S}_i\cdot\mathbf{S}_j\right)\left[\frac{1}{4}+T_i^{\zeta}T_j^{\zeta}-\frac{1}{2}(T_i^{-}T_j^{-}+T_i^{-}T_j^{-})\right] \\
& -\frac{4t^2}{U+J'}\left(\frac{1}{4}-\mathbf{S}_i\cdot\mathbf{S}_j\right)\left[\frac{1}{4}+T_i^{\zeta}T_j^{\zeta}+\frac{1}{2}(T_i^{+}T_j^{+}+T_i^{-}T_j^{-})\right],
\end{aligned} \tag{3}$$

where $\mathbf{S}_i=(1/2)\Sigma_{\gamma\sigma\sigma'} d_{i,\gamma\sigma}^{\dagger} \boldsymbol{\sigma}_{\sigma\sigma'} d_{i,\gamma\sigma'}$ is the $S=1/2$ spin op-

erator ($\boldsymbol{\sigma}$ is the Pauli matrix), and we define the $T=1/2$ pseudospin operator representing the xy and zx orbitals as $\mathbf{T}_i=(1/2)\Sigma_{\gamma\gamma'\sigma}d^{\dagger}_{i,\gamma\sigma}\boldsymbol{\sigma}_{\gamma\gamma'}d_{i,\gamma'\sigma}$. Note that this effective model has $SU(2)$ symmetry for the spin degree of freedom and $U(1)$ symmetry for the orbital degree of freedom, since H_{eff} commutes with $\Sigma_i\mathbf{S}_i$ and $\Sigma_i T^y_i$, respectively. On the other hand, when $J=J'=0$, there exists an extra $SU(4)$ symmetry involving both spin and orbital degrees of freedom. The properties of such an $SU(4)$ spin-orbital model have recently been investigated intensively,[17–19] to clarify the combined quantum effects of spin and orbital. Concerning a less symmetric case than $SU(4)$, the effect of J has also been discussed,[20–22] but the effect of J' was not included. If we simply set $J'=0$ and $U=U'$ and consider finite J in the present case, the effective Hamiltonian of Eq. (3) certainly reproduces the equivalent form given in previous works.[20–22]

B. Spin correlations at several densities

To understand more quantitatively the magnetic order present in the PM phase, it is useful to measure the spin-spin correlation function,

$$C_{\text{spin}}(l)=\frac{1}{M}\sum_{|i-j|=l}\langle S^z_i S^z_j\rangle, \tag{4}$$

where $S^z_i=\Sigma_\gamma(\rho_{i\gamma\uparrow}-\rho_{i\gamma\downarrow})/2$ is the z component of the total spin at each site and M is the number of site pairs (i,j) satisfying $l=|i-j|$. We average over all pairs of sites separated by distance l in order to minimize boundary effects. In Fig. 3(a), C_{spin} is shown for the PM phase. Assuming the behavior of the Tomonaga-Luttinger liquid,[23] which is characteristic of one-dimensional strongly correlated systems, we apply the following fitting function:

$$\tilde{C}_{\text{spin}}(j)=\frac{a}{j^2}+b\frac{\cos\left(\frac{\pi}{2}j\right)}{j^{3/2}}, \tag{5}$$

where a and b are appropriate fitting parameters. As shown by the dashed curve, we find that the numerical data of C_{spin} are well reproduced by $\tilde{C}_{\text{spin}}$. The result indicates that the spin-spin correlation function has a four-site periodicity and decays as a power law with critical exponent 3/2.[24] These results are consistent with previous analytical work[25] and numerical investigations[17,21] for the $SU(4)$ spin-orbital model. In the inset of Fig. 3(a), we also present the Fourier transform of the spin-spin correlation function,

$$S(q)=\frac{1}{L}\sum_{j,k}e^{iq(j-k)}\langle S^z_j S^z_k\rangle, \tag{6}$$

for $L=16$ and $L=48$. We clearly observe a peak in $S(q)$ at $q=\pi/2$, corresponding to the four-site periodicity of the spin-spin correlation function. Note that although finite-size effects appear to be very small, the peak height increases for larger L, indicating the development of the spin correlation of $q=\pi/2$ in these system sizes.

As shown in the linear-log scale in Fig. 3(b), the spin-spin correlation function for $n=5$ clearly present distinct behavior

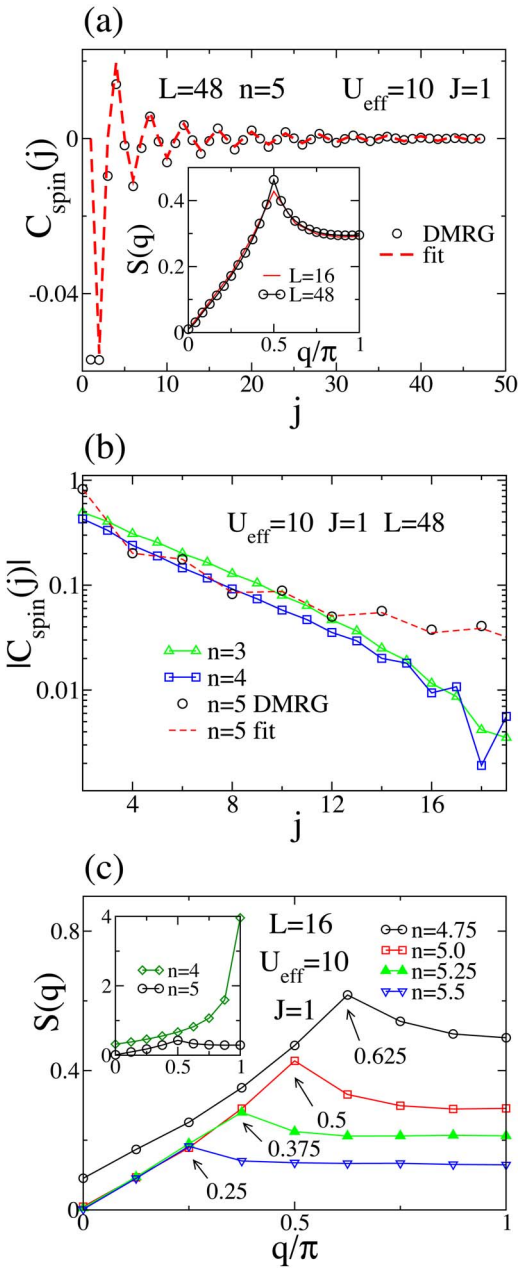

FIG. 3. (Color online) (a) The spin-spin correlation function $C_{\text{spin}}(j)$ vs j for $L=48$ and density $n=5$. The dashed curve indicates a fit using Eq. (5). The inset shows the spin structure factor $S(q)$ for $L=16$ and $L=48$. (b) The linear-log plot of the module of the spin-spin correlation function $|C_{\text{spin}}(l)|$ for densities $n=3$, 4, and 5 with $L=48$, as well as the fit used in (a). For details, see the main text. (c) The spin structure factor $S(q)$ for several densities n, and using $L=16$. The arrows indicate the peak positions. In all plots $U_{\text{eff}}=10$ and $J=1$, as indicated. Inset shows $S(q)$ for $n=4$ and 5.

from the results already reported for $n=4$.[15] For better comparison, we have normalized C_{spin} in such a way that the correlations are the same at distance 1. We have eliminated the odd sites for $n=5$, since the results there are close to zero [see Fig. 3(a)]. Moreover, working with $m=350$, it is difficult to reach good accuracy for the correlations at large distances, since they are very small. For this reason, we show the results only for the first 19 sites. Here we stress that for $n=5$,

the power-law decaying correlation indicates a *gapless* spin-excitation spectrum,[26] in contrast to a gapful behavior for $n=4$. We note that to confirm the quantum critical behavior, it is necessary to clarify the decaying behavior of the spin correlation at further long distances, for instance, using the effective two-orbital model composed of xy and zx orbitals. This level of detailed analysis is left for future investigations.

In Fig. 3(b), we also show the spin-spin correlation function for $n=3$. In the case of $n=3$, it is naively expected that a local spin $S=3/2$ is formed at each site. By analogy with the half-odd-integer-spin antiferromagnetic Heisenberg chains, we expect a power-law decay of the spin-spin correlation function and a gapless spin-excitation spectrum as well.[27] On the contrary, we can observe in Fig. 3(b) that the spin-spin correlation function shows an exponential decay similar to the case for the integer-spin chains. To understand this peculiar behavior, it is necessary to take into account the effect of t_{2g} orbitals. As mentioned above, electrons in the yz orbital cannot hop, whereas electrons in the xy and zx orbitals move to adjacent sites with the same amplitude. Then, it is expected that only electrons in the xy and zx orbitals contribute to the exchange interaction, and the $n=3$ system is, thus, better regarded as an effective $S=1$ chain, leading to the exponential decaying spin-spin correlation function.[28]

In Fig. 3(c), $S(q)$ is shown for several densities. Since the finite-size effects seem to be small, we consider $L=16$. As observed in these studies, the results suggest that the peak position changes linearly with the electron density as $q=(6-n)\pi/2 \pmod{\pi}$. Note that this peak is clearly robust for $n=4$, as shown in the inset of Fig. 3(c), and substantially decreases its intensity by increasing the density n.

It is important to remark that the inset of Fig. 3(a) is very similar to the results found by Ogata and Shiba in their study of the one-dimensional Hubbard model at quarter-filling and $U=\infty$ (see Fig. 9 of Ref. 29). Clearly, in the model studied in this paper, the electrons in the two bands with a nonzero hopping behave like one-band models with a strong on-site repulsion, at least from the perspective of the spin correlations. Note, however, that these two one-band models are connected via the Coulombic repulsion, which, as discussed below, will open a gap in the spectrum of charge excitations.

C. Charge correlations at several densities

To investigate the charge excitations, it is useful to measure the charge gap, defined as $\Delta=E(N_e+2)+E(N_e-2)-2E(N_e)$, where $E(N_e)$ denotes the lowest energy in the subspace with the total number of electrons N_e. In Fig. 4(a), the charge gap is shown as a function of $1/L$ at densities $n=4$ and 5, for particular values of U_{eff} and J. Clearly, at these densities the charge gap extrapolates to a nonzero value in the thermodynamic limit, indicating that the system is an *insulator*. On the other hand, as shown in Fig. 4(b), for noninteger electron densities, the charge gaps seem to extrapolate to zero in the thermodynamic limit, suggesting a metallic behavior. These results indicate that a transition from an insulating phase to a metallic regime is obtained by changing the density away from $n=5$.

In Fig. 4(c), the charge gap for the density $n=5$ and $L=12$ is presented. It appears that U' is the main driver of the

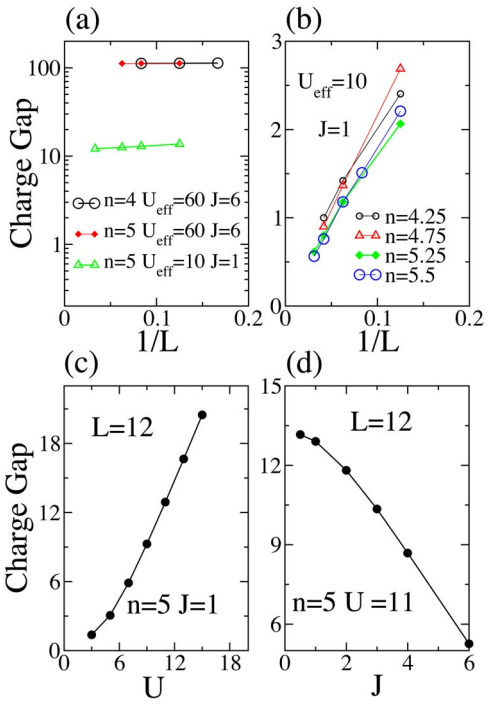

FIG. 4. (Color online) (a) The charge gap Δ vs $1/L$ at particular values of U_{eff} and J, and densities $n=4$ and $n=5$. (b) Same as (a) but for noninteger densities, and $U_{\text{eff}}=10$ and $J=1$. (c) and (d) denote the charge gap for density $n=5$ and $L=12$. (c) contains Δ vs U' at $J=1$, while (d) shows Δ as a function of J at $U'=11$.

system into an insulating phase. On the other hand, the Hund's coupling J has the opposite effect, as observed in Fig. 4(d). Namely, the charge gap decreases with increasing J. Note that U' plays a role similar to that of the nearest-neighbor Coulomb repulsion V in the two-leg ladder extended Hubbard model (with the two legs playing the role of the two orbitals in our model). In the ladder case, it is known that V drives the system to an insulator at quarter-filling.[30]

We have also investigated the charge structure factor, defined as

$$N^{\gamma,\gamma'}(q)=\frac{1}{2L}\sum_{j,k} e^{iq(j-k)}[N^{\gamma,\gamma'}(j,k)+N^{\gamma',\gamma}(j,k)], \qquad (7)$$

where $N^{\gamma,\gamma'}(j,k)=\langle \delta n_\gamma(j)\,\delta n_{\gamma'}(k)\rangle$ and $\delta n_\gamma(j)=n_\gamma(j)-\langle n_\gamma(j)\rangle$. In a periodic system, $N^{\gamma,\gamma'}(j,k)=N^{\gamma',\gamma}(j,k)$. However, with open boundary conditions, as used in our investigation, this is no longer valid because of the presence of Friedel oscillations. Using the definition discussed above, $N^{\gamma,\gamma'}(q=0)$ is always *zero*. In our calculations, we obtained $N^{\gamma,\gamma'}(q=0)<10^{-4}$, indicating that we have retained enough states in the truncation process to satisfy this constraint.

The best indication of a true long-range order (LRO) can be obtained by the system-size dependence of $N^{\gamma,\gamma'}(q)$. If $N^{\gamma,\gamma'}(q^*)/L\to$ constant as $L\to\infty$, at some particular q^*, a true LRO characterized by q^* is present. Carrying out this analysis, we have found no evidence of LRO in the charge sector of $n=5$. In Figs. 5(a), 5(c), and 5(e), typical examples of the

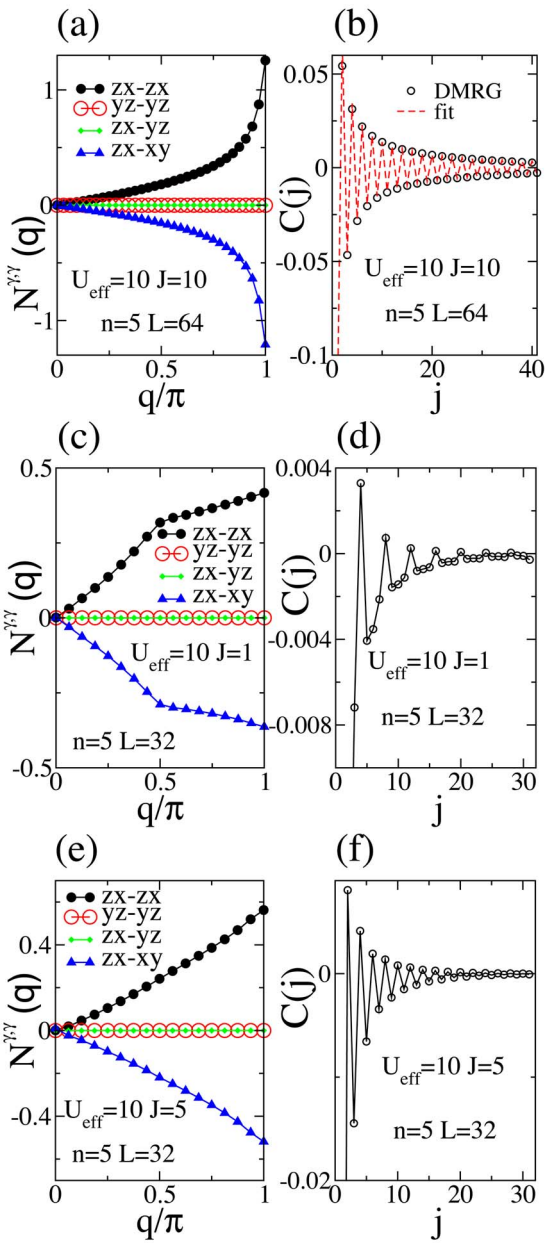

FIG. 5. (Color online) The charge structure factor $N^{\gamma,\gamma'}(q)$ and the charge-charge correlation function $C(j)$, at density $n=5$. (a) and (b) are for $U_{\text{eff}}=10$, $J=10$, and $L=64$. This corresponds to the FM regime of Fig. 1. The dashed curve is a fit using the function $a\cos(\pi j)/j$ with an appropriate fitting parameter a. (c) and (d) are for $U_{\text{eff}}=10$, $J=1$, and $L=32$. This is in the PM regime of Fig. 1. (e) and (f) are the same as (c) and (d), respectively, but for $J=5$.

charge structure factor for the FM and PM phases at density $n=5$ are presented. In the FM phase, we are able to explore very large system sizes, since we can measure the correlations in the sector of $S^z_{\text{total}}=\max$, with a much smaller Hilbert space than for the PM phase. Although we did not find LRO, the behavior of the structure factor suggests that in the FM phase the charge-charge correlation presents a quasi LRO due to the presence of a robust peak at $q=\pi$. In fact, in the charge-charge correlation function, defined as

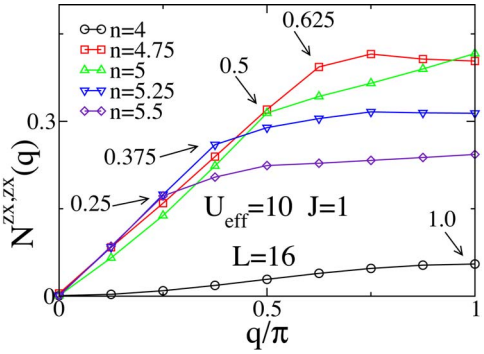

FIG. 6. (Color online) The charge structure factor $N^{zx,zx}(q)$ for several densities and using $U_{\text{eff}}=10$, $J=1$, and $L=16$. The arrows indicate the cusp positions.

$$C(l)=\frac{1}{M}\sum_{|i-j|=l}\langle \delta n_{zx}(i)\,\delta n_{zx}(j)\rangle, \tag{8}$$

we observe a slow power-law decay, as shown in Fig. 5(b). This correlation oscillates as $\cos(\pi j)/j$, as indicated by the dotted curve in Fig. 5(b). The DMRG data agree very nicely with a fit using this function.

Note also that the negative values of $N^{zx,xy}(q=\pi)$ suggest an alternation of charge occupation between the zx and xy orbitals, as in the schematic representation in Fig. 1 (FM phase). Indeed, as discussed later in more detail, there is quasi-long-range AFO order. A similar result has already been found in the FM phase for the density $n=4$.[15]

On the other hand, in the PM phase, $N^{\gamma,\gamma'}(q)$ does not present a peak as sharp as for the FM phase, as shown in Fig. 5(c). In fact, the magnitude of the charge correlations is drastically different between the PM and FM phases, as can be seen from the absolute values of these correlations in the vertical axes of Figs. 5(b) and 5(d). Note that the appearance of the cusp at $q=\pi/2$ is related to the four-site periodicity of the correlation $C(l)$, as shown in Fig. 5(d).

Our results also suggest that the charges behave differently in two distinct regimes in the PM phase. At small J, the correlation $C(l)$ presents a four-sites periodicity, while for larger J, only a two-site periodicity is found, as observed in Fig. 5(f). In addition, the cusp of $N^{zx,zx}(q)$ present in the small-J regime disappears at larger J [Fig. 5(e)], apparently continuously. We have also observed that at small J, the position of the cusp changes with the electron density in a similar way as $S(q)$, as shown in Fig. 6.

D. Orbital correlations at $n=5$

Consider now the possibility of orbital order. In the PM phase at $n=5$, we have found that the xy and zx orbitals are those of relevance, since the yz orbitals are fully occupied. Note that in the PM phase at $n=4$, the orbital degree of freedom becomes inactive due to the ferro-orbital order.[15] Then, here we take the pseudospin representation for the xy and zx orbitals, and measure the orbital correlations to determine the orbital structure. For this purpose, we introduce an angle θ_j to characterize the orbital shape at each site. Using

the angle θ_j, we define the phase-dressed operators as

$$\begin{cases} f_{j,a,\sigma} = e^{i\theta_j/2}[\cos(\theta_j/2)d_{j,xy,\sigma} + \sin(\theta_j/2)d_{j,zx,\sigma}], \\ f_{j,b,\sigma} = e^{i\theta_j/2}[-\sin(\theta_j/2)d_{j,xy,\sigma} + \cos(\theta_j/2)d_{j,zx,\sigma}]. \end{cases} \quad (9)$$

The optimal orbitals, a and b, are determined so as to maximize the orbital structure factor, defined as

$$T(q) = \frac{1}{L}\sum_{j,k} e^{iq(j-k)}\langle T^z(i)T^z(j)\rangle, \quad (10)$$

where $T^z(j) = \Sigma_\sigma(f^\dagger_{j,a,\sigma}f_{j,a,\sigma} - f^\dagger_{j,b,\sigma}f_{j,b,\sigma})/2$.

Let us first focus on the case $\theta_i = \theta = 0$. In Figs. 7(a) and 7(c), typical examples of the orbital structure factor in the FM and PM phases at density $n=5$ are presented. Note that these results are similar to those of the charge structure factor shown in Figs. 5(a) and 5(c), as previously anticipated. Also, as shown in Figs. 7(b) and 7(d), concerning the orbital correlation function defined as

$$C_{\text{orbital}}(l) = \frac{1}{M}\sum_{|i-j|=l} \langle T^z(i)T^z(j)\rangle, \quad (11)$$

we find the same form as $C(l)$, as observed in Figs. 5(b) and 5(d). In the FM phase, as shown in Fig. 7(b), $C_{\text{orbital}}(l)$ decays as $\cos(\pi j)/j$, which is the signature of quasi-long-range AFO. On the other hand, in the PM phase, we observe a four-site periodicity of $C_{\text{orbital}}(j)$ as well as that of $C_{\text{spin}}(j)$, while the peak position of $T(q)$ is at $q=\pi$ for $U_{\text{eff}}=10$ and $J=1$. Note that the spin-spin correlation function shows the four-site periodicity and $S(q)$ has the peak at $q=\pi/2$ for $U_{\text{eff}}=10$ and $J=1$, as shown in Fig. 3(a).

To clarify the similarity between the two-orbital model composed of the xy and zx orbitals and the $SU(4)$ spin-orbital model, we investigate $C_{\text{spin}}(l)$ and $C_{\text{orbital}}(l)$ for the present t_{2g} model, at $U_{\text{eff}}=10$ and $J=0$. As shown in Figs. 7(e) and 7(f), it is clearly observed that $C_{\text{orbital}}(l)$ and $C_{\text{spin}}(l)$ present exactly the same behavior with a four-site periodicity, due to the presence of the $SU(4)$ symmetry at $J=0$. When we include the effect of J, the spin and orbital degrees of freedom are no longer equivalent, but we can observe the four-site periodicity in both $C_{\text{orbital}}(l)$ and $C_{\text{spin}}(l)$ due to the influence of the $SU(4)$ symmetry at $J=0$. Thus, the short-range orbital correlation for small J originates in the $SU(4)$ singlet at $J=0$.

It should be mentioned that there is no indication of orbital LRO in the PM phase, since $T(\pi)$ converges to a finite value in the thermodynamic limit, as shown in Fig. 8(a). On the other hand, although we have found no signature of orbital order between the xy and zx orbitals through the orbital structure factor $T(q)$ for $\theta_i=\theta=0$, a more complex combination between these orbitals could exist, but we cannot observe it directly from $T(q)$ with $\theta=0$. In order to consider other combinations, we set $\theta_i=\theta$ and change the value of θ. However, even in this case, we do not observe any changes in $T(q)$, as observed in Fig. 8(b). Namely, the orbital correlation does not change because of the rotation in the orbital space, and we cannot determine the optimal orbitals. Note that even if we optimize θ_i at each site, $T(\pi)$ is always maximum. Thus, we conclude that the states considered in our investigations do not have long-range orbital order in the PM phase.

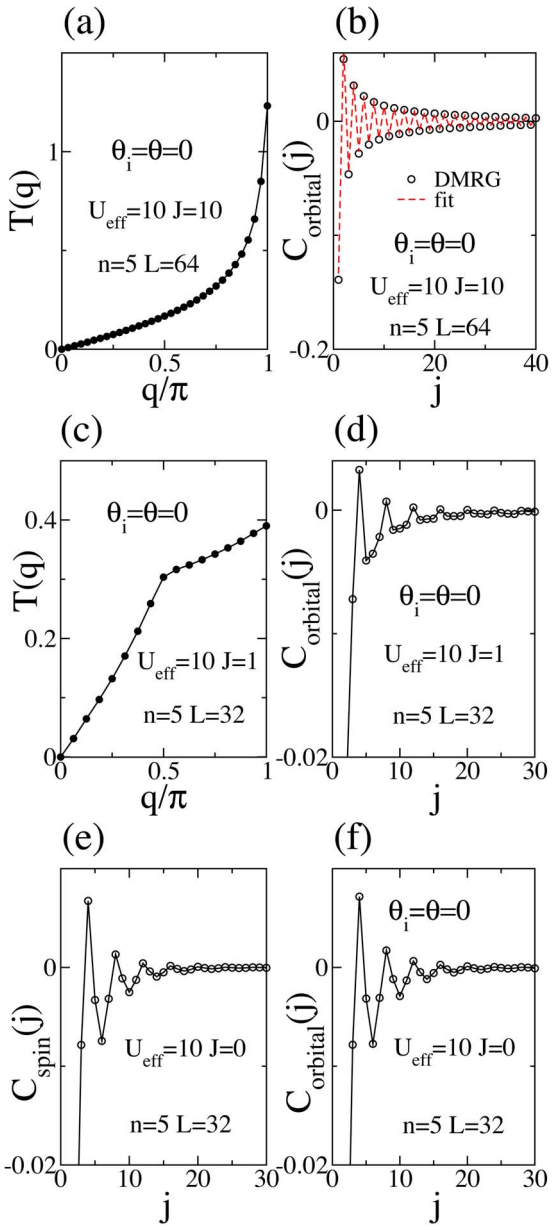

FIG. 7. (Color online) (a) The orbital structure factor $T(q)$ versus momentum for $U_{\text{eff}}=10$, $J=10$, and $L=64$ with $\theta_i=\theta=0$. (b) The orbital correlation $C_{\text{orbital}}(j)$ for the same parameters as used in (a). The dashed curve is a fit using the function $a\cos(\pi j)/j$. (c) and (d) are the same as (a) and (b), but for $U_{\text{eff}}=10$, $J=1$, and $L=32$. (e) and (f) contain the correlations $C_{\text{spin}}(j)$ and $C_{\text{orbital}}(j)$ for $U_{\text{eff}}=10$, $J=0$, and $L=32$. All the results are for the density $n=5$.

IV. CONCLUSIONS

In this paper, we have investigated the properties of the one-dimensional Hubbard model with three active orbitals, with emphasis on electron densities of relevance for Co oxides. We envision this work as a step toward a numerically

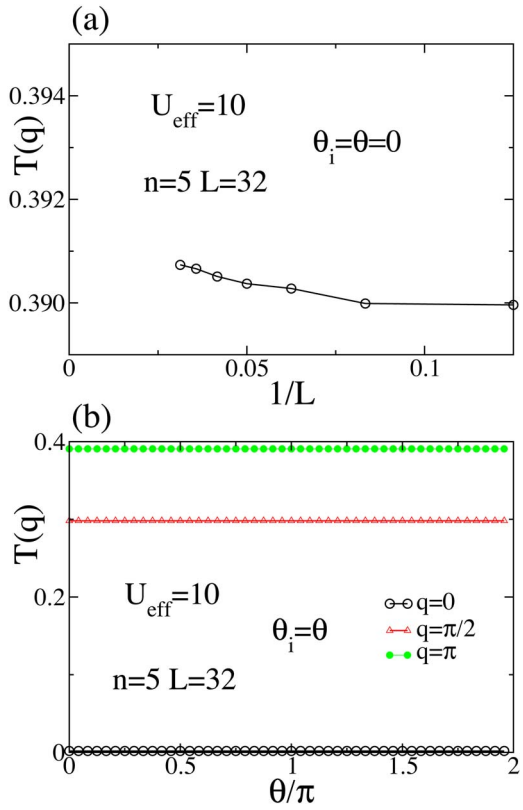

FIG. 8. (Color online) (a) The size dependence of the orbital structure factor $T(q)$ at $q=\pi$ with $\theta_i=\theta=0$, at density $n=5$. (b) $T(q)$ vs θ for particular values of q.

accurate study of many-body Hamiltonians for Co oxides, including the Coulombic repulsion. Our main result is the identification of two dominant ground-state tendencies: PM with robust short-range correlations and FM states. We believe that the ferromagnetic tendencies experimentally identified in the quasi-one-dimensional material $BaCoO_3$, as discussed in the introduction, could be explained by the FM state found in our investigation. Other quasi-one-dimensional Co oxides could exist with Coulomb repulsion parameters favoring the PM state, and experimental efforts trying to find this state would be extremely interesting.

To the extent that our results can be qualitatively extended to higher dimensions, the main competition in Co-oxide models should originate from these FM and PM states. In the FM phase, there exists strong charge oscillations. Then, it is naively expected that true long-range charge order would develop in higher dimensions. However, it is necessary to consider that the hopping term depends on the dimensionality and the lattice structure. Namely, the *yz* orbital is localized for the present case, but this will not occur in higher-dimensional systems, in general. Thus, due care should be paid to extend the present discussions to higher dimensions. On the other hand, the PM state has short-range correlations in all channels, and in some limits it has an extra $SU(4)$ symmetry as in previously studied two-orbital models. Although this exact symmetry may appear only in one dimension and for $J=0$, it would be interesting to investigate whether remnants survive under more realistic conditions.

Of course, the effect of geometrical frustration could be also an important ingredient to influence on the complex spin-charge-orbital structure of the triangular-lattice systems. In fact, two of the authors have revealed that the spin frustration is suppressed because of the orbital ordering in the e_g-orbital model on a zigzag chain.[31] In addition, in the present work we have identified metal-insulator transitions with doping away from $n=5$, while the main properties in the spin and charge sectors remain similar as for the integer density $n=5$. The next challenge is to increase the dimensionality of the t_{2g} system toward two dimensions by studying ladders and/or zigzag chains. Work is in progress in this direction.

ACKNOWLEDGMENTS

This work was supported by Grant No. DMR-0454504 (E.D. and J.C.X.) and Grant No. FAPESP-04/09689-2 (J.C.X.). T. H. is supported by the Japan Society for the Promotion of Science and by the Ministry of Education, Culture, Sports, Science, and Technology of Japan.

[1] K. Takada, H. Sakurai, E. Takayama-Muromachi, F. Izumi, R. A. Dilanian, and T. Sasaki, Nature (London) **422**, 53 (2003); R. E. Schaak, T. Klimczuk, M. L. Foo, and R. J. Cava, *ibid.* **424**, 527 (2003).

[2] Y. Wang, N. S. Rogado, R. J. Cava, and N. P. Ong, Nature (London) **423**, 425 (2003); T. Motohashi, R. Ueda, E. Naujalis, T. Tojo, I. Terasaki, T. Atake, M. Karppinen, and H. Yamauchi, Phys. Rev. B **67**, 064406 (2003).

[3] J. Sugiyama, H. Itahara, T. Tani, J. H. Brewer, and E. J. Ansaldo, Phys. Rev. B **66**, 134413 (2002); J. Sugiyama, J. H. Brewer, E. J. Ansaldo, B. Hitti, M. Mikami, Y. Mori, and T. Sasaki, *ibid.* **69**, 214423 (2004).

[4] E. Dagotto, Science **309**, 257 (2005).

[5] J. Sugiyama, H. Nozaki, J. H. Brewer, E. J. Ansaldo, T. Takami, H. Ikuta, and U. Mizutani, Phys. Rev. B **72**, 064418 (2005).

[6] V. Pardo, P. Blaha, M. Iglesias, K. Schwarz, D. Baldomir, and J. E. Arias, Phys. Rev. B **70**, 144422 (2004).

[7] D. J. Singh, Phys. Rev. B **68**, 020503(R) (2003).

[8] N. Bulut, W. Koshibae, and S. Maekawa, Phys. Rev. Lett. **95**, 037001 (2005), and references therein.

[9] M. Mochizuki, Y. Yanase, and M. Ogata, J. Phys. Soc. Jpn. **74**, 1670 (2005), and references therein.

[10] M. Ogata, J. Phys. Soc. Jpn. **72**, 1839 (2003); G. Baskaran, Phys. Rev. Lett. **91**, 097003 (2003); B. Kumar and B. S. Shastry, Phys. Rev. B **68**, 104508 (2003), and references therein.

[11] H. Ikeda, Y. Nisikawa, and K. Yamada, J. Phys. Soc. Jpn. **73**, 17 (2004); Y. Nishikawa, H. Ikeda, and K. Yamada, *ibid.* **73**, 1127 (2004).

[12] S. R. White, Phys. Rev. Lett. **69**, 2863 (1992).

[13] E. Dagotto, Rev. Mod. Phys. **66**, 763 (1994).

[14] E. Dagotto, T. Hotta, and A. Moreo, Phys. Rep. **344**, 1 (2001); E. Dagotto, *Nanoscale Phase Separation and Colossal Magnetoresistance* (Springer-Verlag, Berlin, 2002).
[15] H. Onishi and T. Hotta, Phys. Rev. B **70**, 100402(R) (2003).
[16] Y. Q. Li, M. Ma, D. N. Shi, and F. C. Zhang, Phys. Rev. Lett. **81**, 3527 (1998).
[17] B. Frischmuth, F. Mila, and M. Troyer, Phys. Rev. Lett. **82**, 835 (1999).
[18] Y. Yamashita, N. Shibata, and K. Ueda, Phys. Rev. B **61**, 4012 (2000).
[19] C. Itoi, S. Qin, and I. Affleck, Phys. Rev. B **61**, 6747 (2000).
[20] D. P. Arovas and A. Auerbach, Phys. Rev. B **52**, 10114 (1995).
[21] Y. Yamashita, N. Shibata, and K. Ueda, Phys. Rev. B **58**, 9114 (1998).
[22] H. C. Lee, P. Azaria, and E. Boulat, Phys. Rev. B **69**, 155109 (2005).
[23] J. Voit, Rep. Prog. Phys. **57**, 977 (1994).
[24] Actually, it is expected that this exponent 3/2 will depend on U, J, and the density n. Here, we do not intend to present a systematic study of this exponent. Our intention is only to show that at large U, it has the same exponent as the $SU(4)$ model. Note also the similarity with the 1D Hubbard model, where this exponent for $U\rightarrow\infty$ is also 3/2 (see, for example, Ref. 23).
[25] I. Affleck, Nucl. Phys. B **265**, 409 (1986).
[26] In Ref. 22, by using renormalization-group and bosonization analyses, Lee *et al.* suggested that the $SU(4)$ system immediately becomes spin gapful for finite J, on the basis of the $SU(4)$ model with an extra term denoting the Hund's rule coupling. In order to relate such a model to our Hamiltonian for orbital degenerate systems, it is necessary to set J as a free parameter with $U=U'$ and $J'=0$, but this condition is different from standard ones, $U=U'+J+J'$, $J'=J$, and $U'>J$. Thus, in our investigations it is quite natural to arrive at the phase diagram (Fig. 1), which is different from that in Ref. 22. Concerning the effect of the Hund's rule coupling, it is necessary for us to confirm whether the spectral gap converges to zero or a small but finite value in the thermodynamic limit, by calculating in even more detail the system-size dependence of the gap. This is left as a future problem.
[27] F. D. M. Haldane, Phys. Lett. **93A**, 464 (1983); Phys. Rev. Lett. **50**, 1153 (1983).
[28] Note that we tried to calculate directly the finite spin gap anticipated from the $n=3$ and 4 results. However, this is a difficult task, since even for small systems the spin gap is already very small ($<10^{-2}$).
[29] M. Ogata and H. Shiba, Phys. Rev. B **41**, 2326 (1990).
[30] S. Daul and R. M. Noack, Phys. Rev. B **58**, 2635 (1998).
[31] H. Onishi and T. Hotta, Phys. Rev. B **71**, 180410(R) (2005).